Title: A bright and high-performance genetically encoded Ca^{2+} indicator based on mNeonGreen fluorescent protein

Authors: Landon Zarowny[1] (equal contribution), Abhi Aggarwal[1,2] (equal contribution), Virginia Rutten[2,3], Ilya Kolb[2], The GENIE Project[2], Ronak Patel[2], Hsin-Yi Huang[4], Yu-Fen Chang[4], Tiffany Phan[1], Richard Kanyo[5], Misha Ahrens[2], W. Ted Allison[5], Kaspar Podgorski[2], Robert E. Campbell[1,6]

Affiliations

[1]Department of Chemistry, University of Alberta, Edmonton, Alberta, Canada

[2]Janelia Research Campus, Howard Hughes Medical Institute, Ashburn, Virginia, United States

[3]Gatsby Computational Neuroscience Unit, UCL, London, UK

[4]LumiSTAR Biotechnology, Inc. National Biotechnology Research Park, Taipei City 115, Taiwan

[5]Department of Biological Sciences, University of Alberta, Edmonton, Alberta, Canada

[6]Department of Chemistry, Graduate School of Science, The University of Tokyo, Tokyo, Japan

Abstract

Genetically encodable calcium ion (Ca^{2+}) indicators (GECIs) based on green fluorescent proteins (GFP) are powerful tools for imaging of cell signaling and neural activity in model organisms. Following almost two decades of steady improvements in the *Aequorea victoria* GFP (avGFP)-based GCaMP series of GECIs, the performance of the most recent generation (i.e., GCaMP7) may have reached its practical limit due to the inherent properties of GFP. In an effort to sustain the steady progression towards ever-improved GECIs, we undertook the development of a new GECI based on the bright monomeric GFP, mNeonGreen (mNG). The resulting indicator, mNG-GECO1, is 60% brighter than GCaMP6s *in vitro* and provides comparable performance as demonstrated by imaging Ca^{2+} dynamics in cultured cells, primary neurons, and *in vivo* in larval zebrafish. These results suggest that mNG-GECO1 is a promising next-generation GECI that

could inherit the mantle of GCaMP and allow the steady improvement of GECIs to continue for generations to come.

Introduction

Genetically encodable calcium ion (Ca^{2+}) indicators (GECIs) are a class of single fluorescent protein (FP)-based biosensors that are powerful tools for the visualization of Ca^{2+} concentration dynamics both *in vitro* and *in vivo*[1, 2, 3]. As they are genetically encoded, GECI expression can be genetically targeted to specific cell types or subcellularly localized to specific organelles. Furthermore, their negligible cellular toxicity, minimal perturbation of endogenous cellular functions, and biological turnover, make them ideal for long-term imaging experiments[4]. The Ca^{2+}-dependent fluorescent response of GECIs is routinely used as a proxy for neuronal activity due to the transient changes in Ca^{2+} concentration that accompany action potentials[5, 6, 7, 8]. GECIs have facilitated the optical recording of thousands of neurons simultaneously in the surgically exposed brains of mice[9]. Despite their widespread use by the scientific community, there are some properties of GECIs that could be further improved. These properties include faster Ca^{2+} response kinetics, higher fluorescent molecular brightness, and minimized contribution to Ca^{2+} buffering. Some GECIs have shown aggregation in neurons, and some of the most highly optimized GECIs have been demonstrated to cause aberrant cortical activity in murine models[10, 11, 12].

An important issue that is common to all GECIs is their intrinsic Ca^{2+} buffering capacity. The Ca^{2+} binding domains of GECIs (calmodulin (CaM) or troponin C (TnC)) act as Ca^{2+} buffers within the cell and must necessarily compete with endogenous proteins for binding to Ca^{2+} (Refs. 13, 14, 15, 16). Comprehensive investigations of this phenomenon are limited, but a few reports have indicated abnormal morphology and behavior of neurons after long term or high expression of GCaMPs[17]. Ca^{2+} buffering and competition for CaM binding sites have been proposed as possible causes. One solution to the Ca^{2+} buffering phenomenon is to reduce the reporter protein expression, leading to a lower concentration of GECI and reduced buffering capacity. However, reduced expression requires increased intensity of excitation light to achieve an equivalent fluorescent signal, which can lead to increased phototoxicity and photobleaching. Another solution is to reduce the number of Ca^{2+} binding sites like that in the TnC-based GECIs, NTnC[18] and YTnC[19]. Unfortunately, these indicators have relatively low fluorescence response ($\Delta F/F_{min}$ ~ 1 for NTnC and ~ 10.6 for YTnC) compared to the recent GCaMP7 variants ($\Delta F/F_{min}$ ~ 21 to 145)[20]. Another possible solution is to develop GECIs with increased brightness such that they could be

expressed at a lower concentration while retaining a similar fluorescent intensity with similar intensity of excitation light.

Further increasing the brightness of GECIs, while retaining high performance comparable to the most recent generation of indicators, would provide improved tools for optical imaging of neuronal activity and decrease the occurrence of experimental artifacts resulting from Ca^{2+} buffering and indicator overexpression[17]. Our efforts to realize this advance were inspired, in part, by the advent of a bright and monomeric engineered version of GFP from *Branchiostoma lanceolatum*, mNeonGreen (mNG)[21]. Due to its high brightness and its excellent performance as a subcellular localization tag[21], mNG is an exceptionally promising starting point from which to develop a brighter GECI.

Here we introduce an mNG-based genetically encodable Ca^{2+} indicator for optical imaging (mNG-GECO1) that exceeds the brightness of all variants in the GCaMP series while providing performance that is comparable to the latest generation GCaMP variants. Key design differences between mNG-GECO1 and the GCaMP series include the GFP portion (mNG versus avGFP) and the protein topology (non-circularly permuted mNG versus circularly permuted avGFP).

Results and Discussion

Rational engineering and iterative directed evolution of mNG-GECO1

We used a combination of rational design, linker sequence optimization, and directed evolution to develop mNG-GECO1 (**Supplementary Fig. 1**). Starting from an unpublished topological variant of REX-GECO1[22], we used PCR to produce a fragment containing CaM linked to the RS20 peptide with a short linker (**Fig. 1a**). Insertion of this PCR fragment into the mNG gene between residues 136 and 137 (numbering as in PDB ID 5LTR)[23] resulted in a green fluorescent indicator prototype which we named mNG-GECO0.1 (**Fig. 1**). For the remainder of this manuscript, amino acids will be numbered as in the sequence alignment provided as **Supplementary Fig. 2**. mNG-GECO0.1 had a minimal response to Ca^{2+} ($\Delta F/F_{min}$ = 0.3), but we anticipated that optimization of the sequence around the insertion site would yield a suitable template for directed evolution. Indeed, we found that deletion of Ala146, the residue immediately preceding the insertion of the Ca^{2+} sensing domain, substantially improved the response to Ca^{2+} (mNG-GECO0.2; $\Delta F/F_{min}$ ~ 2).

88 Starting from mNG-GECO0.2, we began a process of iterative directed evolution which
89 involved screening of libraries created from error-prone PCR or site saturation mutagenesis to
90 identify variants with increased brightness and increased response to Ca^{2+}. In our primary library
91 screen, we used a fluorescent colony screening system equipped with excitation and emission
92 filters appropriate for imaging of green fluorescence[24]. Bright colonies were picked and cultured
93 overnight in liquid media. A secondary screen for Ca^{2+} sensitivity was performed the next day
94 using detergent-extracted bacterial lysate. The fluorescence of the lysate for each variant was
95 measured in Ca^{2+} chelating buffer (30 mM MOPS, 100 mM KCl, 10 mM EGTA, pH 7.3), and
96 subsequently in Ca^{2+} saturating buffer (30 mM MOPS, 100 mM KCl, 10 mM Ca^{2+}, pH 7.3). Dividing
97 the Ca^{2+} saturated fluorescence by the Ca^{2+} free fluorescence provided an approximate but robust
98 measure of each indicator variant's response to Ca^{2+}. For each round of screening the plasmids
99 were isolated for the 6-10 most promising variants and sent for sequencing. The pool of these
100 most promising variants was used as the template for the next round of library creation and
101 directed evolution.

102 Following 7 rounds of iterative directed evolution, *E. coli* colonies harboring mNG-
103 GECO0.7 were brightly fluorescent after overnight incubation. However, the Ca^{2+} response of
104 mNG-GECO0.7 was remained relatively low ($\Delta F/F_{min}$ ~ 5), relative to recent generation GCaMP
105 variants. We anticipated that optimization of the linkers connecting mNG to the CaM-RS20
106 domain (mNG-CaM linker and RS20-mNG linker) could lead to the identification of variants with
107 improved responses. To optimize these linker regions, we used site saturation mutagenesis to
108 produce libraries of all 20 amino acids within the 3 residues connecting mNG to CaM. Individual
109 libraries of Leu133, Thr134, and Ala135 were randomized to all 20 amino acids. If a beneficial
110 mutation was found, the process was repeated for the remaining amino acids until these libraries
111 were exhausted. By screening of these libraries, we identified two mutations of the linker region
112 between mNG barrel and CaM: Ala145Gly and Leu143Ile. This variant, mNG-GECO0.9, had a
113 $\Delta F/F_{min}$ ~ 12 as measured *in vitro*.

114 Following optimization of the mNG-CaM linker, multiple site saturation libraries were
115 created, using the same methodology as the mNG-CaM linker, for the RS20-mNG linker region
116 (residues Glu323, Trp324, Cys325 and Arg326). Screening of these libraries led to the
117 identification of a particularly bright variant with a Cys325Asn mutation. This variant, designated
118 mNG-GECO0.9.1, is brighter than mNG-GECO0.9 but has a decreased response to Ca^{2+} of
119 $\Delta F/F_{min}$ = 3.5. In an effort to improve the performance of mNG-GECO0.9.1, we applied site
120 saturations to positions previously found to be mutated during directed evolution. Screening of

121 these libraries for variants with increased brightness and higher $\Delta F/F_{min}$ led to the identification of
122 a variant with Asp206Gly, Phe209Leu, Pro263Phe, Lys265Ser, Thr346Ile and the reversion of
123 Gly152Glu. This variant was designated as mNG-GECO1. A notable observation from the
124 directed evolution efforts is the minimal number of mutations in the mNG domain. Only 2
125 mutations (Lys128Glu and Thr346Ile) were outside the β-strand in which the Ca^{2+} sensing domain
126 was inserted. In contrast, 3 mutations were localized to the β-strand surrounding the sensing
127 domain insertion site (Leu143Ile/Ala145Gly/Cys325Asn) and 7 mutations were localized to the
128 CaM domain (Thr151Ala/Thr180Cys/Asp206Gly/Phe209Leu/Pro263Phe/Lys265Ser/Ala293Gly).

129 ***In vitro* characterization of mNG-GECO1**

130 We characterized mNG-GECO1, in parallel with GCaMP6s, for direct comparison of biophysical
131 properties measured under identical conditions (**Supplementary Table 1).** We found that the
132 excitation (ex) and emission (em) maxima of the Ca^{2+} saturated states to be 497 nm (ex) and 512
133 nm (em) for GCaMP6s and 496 nm (ex) and 513 nm (em) for mNG-GECO1 (**Fig. 1**). The *in vitro*
134 Ca^{2+} response of mNG-GECO1 ($\Delta F/F_{min}$ = 35) was similar to that of GCaMP6s when tested in
135 parallel ($\Delta F/F_{min}$ = 39). The K_d of mNG-GECO1 (810 nM) is substantially higher than that of
136 GCaMP6s (147 nM). This increase in K_d is consistent with the faster k_{off} kinetics of mNG-GECO1
137 (k_{off} = 1.57 +/- 0.01 s^{-1}) relative to GCaMP6s (k_{off} = 1.06 +/- 0.01 s^{-1}). There was no noticeable
138 difference observed between the k_{on} kinetics of mNG-GECO1 and GCaMP6s with varying
139 concentrations of Ca^{2+} (**Supplementary Fig. 3**).

140 In the Ca^{2+} bound state, mNG-GECO1 has an extinction coefficient of 102,000 $M^{-1}cm^{-1}$
141 and quantum yield of 0.69, giving it an overall brightness (= EC * QY) of 70. This value is similar
142 to the value of 77 previously reported for NTnC[18] and 78% of the brightness of mNG itself
143 (measured by us to be 112,000 $M^{-1}cm^{-1}$ * 0.8 = 90) (**Supplementary Fig. 4**). Under two-photon
144 excitation conditions, both mNG-GECO1 and GCaMP6s have a maximal two-photon cross
145 section at ~ 970 nm and similar action cross-section (AXS) values of 37.22 GM for mNG-GECO1
146 and 38.81 GM for GCaMP6s. However, due to its higher brightness at the single molecule level,
147 the molecular brightness of mNG-GECO1 (21.3) is higher than that of GCaMP6s (16.1) at 15 mW
148 power. Overall, these data indicate the mNG-GECO1 has excellent one-photon and two-photon
149 excitation properties *in vitro*.

150

151 **In vitro characterization in cultured cells and dissociated neurons**

152 To compare the performance of mNG-GECO1 and GCaMP6s in cultured cells, we transfected
153 HeLa cells with mNG-GECO1 in a pcDNA vector (CMV promoter) in parallel with pGP-CMV-
154 GCaMP6s. Using a previously reported protocol[25], Ca^{2+} oscillations were induced by treatment
155 with histamine and fluorescence images were acquired every 10 seconds for 20 minutes. From
156 the intensity versus time data for each cell, $\Delta F/F_0$ for all oscillations of $\Delta F/F_0 > 0.5$ were extracted
157 using a Matlab script. Using these extracted $\Delta F/F_0$ values, average $\Delta F/F_0$ for all oscillations and
158 maximum $\Delta F/F_{0,}$ was computed. The average maximum $\Delta F/F_0$ was calculated by averaging the
159 maximum $\Delta F/F_0$ from each responding cell. In parallel experiments, mNG-GECO1 had an average
160 $\Delta F/F_0 = 4.50 \pm 2.96$ compared to GCaMP6s' $\Delta F/F_0 = 3.48 \pm 2.40$ (**Fig. 1h**). The maximum $\Delta F/F_0$
161 was 16.8 ± 10.5 for mNG-GECO1 and 12.8 ± 6.11 for GCaMP6s. At the end of the 20-minute
162 imaging experiment, the cells were treated with ionomycin/Ca^{2+} to saturate the indicators and
163 induce a fluorescent maximum and then with Ca^{2+} chelator EGTA/ionomycin to deplete Ca^{2+} and
164 produce a fluorescent minimum. For these treatments, $\Delta F/F_{min} = 48.8 \pm 15.1$ for mNG-GECO1
165 and $\Delta F/F_{min} = 16.7 \pm 5.2$ for GCaMP6s. These results were obtained from a data set of 137
166 responding cells with 1624 individual oscillations for mNG-GECO1 and 99 responding cells with
167 687 individual oscillations for GCaMP6s (**Supplementary Table 2**).

168 We next characterized the performance of mNG-GECO1 in dissociated rat cortical
169 neurons alongside GCaMP series indicators GCaMP6s, jGCaMP7s, jGCaMP7b, jGCaMP7c, and
170 jGCaMP7f (**Fig. 2**). Field stimulated neurons expressing mNG-GECO1 had a single action
171 potential (AP) $\Delta F/F_0 = 0.19 \pm 0.04$, slightly lower than that of GCaMP6s ($\Delta F/F_0 = 0.27 \pm 0.09$, **Fig.**
172 **2a**). For 10 APs, performance of mNG-GECO1 was approximately twofold lower than GCaMP6s,
173 with $\Delta F/F_0$ of 1.5 ± 0.19 and 3.1 ± 0.26 for mNG-GECO1 and GCaMP6s, respectively (**Fig. 2b**).
174 At 160 APs, mNG-GECO1 has a $\Delta F/F_0$ of 6.5 ± 0.8, slightly lower than GCaMP6s's $\Delta F/F_0$ of 9.0 ±
175 0.47 (**Fig. 2c**). The baseline brightness of mNG-GECO1 (1,374 ± 31 AU) was comparable to the
176 baseline brightness of GCaMP6s (1,302 ± 6 AU) and jGCaMP7s (1,397 ± 11 AU) (**Fig. 2e**). The
177 signal-to-noise ratio (SNR) of mNG-GECO1 and GCaMP6s are comparable for 1 and 3 AP's (**Fig.**
178 **2f**). For 3 AP stimulation, mNG-GECO1 exhibited a half rise time of 49 ± 1 ms and half decay time
179 of 582 ± 12 ms. Under the same conditions, GCaMP6s exhibited a half rise time of 65 ± 2 ms and
180 a half decay time of 1,000 ± 36 ms. Field stimulated neuron data is summarized in
181 **Supplementary Table 3**. The overall data in cultured neuron suggest that the mNG-GECO1
182 sensor is comparable in signal, kinetics, and baseline brightness to the GCaMP6s sensor.

183 ***In vivo* evaluation of mNG-GECO1**

184 To evaluate mNG-GECO1 for *in vivo* expression in zebrafish neurons, we used a Tol2
185 transposase transgenesis system to deliver mNG-GECO1 or GCaMP6s under a pan-neuronal
186 Elavl3 promoter into zebrafish embryos[26]. We tracked expression of mNG-GECO1 over several
187 days to evaluate the viability of transgenic fish (**Supplementary Fig. 5**). We found no obvious
188 morphological anomalies during larval development stage of zebrafish expressing mNG-GECO1
189 or GCaMP6s.

190 To evaluate the relative performance of mNG-GECO1 and GCaMP6s for imaging of
191 neuronal activity in zebrafish larvae, we used the same transgenesis protocol to produce *Casper*
192 zebrafish lines expressing each indicator (**Fig. 3**). Prior to imaging, 5-6 days post fertilization
193 *Casper* fish expressing the sensors were immobilized with bungarotoxin (1 mg/mL) for 30 seconds
194 followed by a 10 minute incubation in the convulsant 80 mM 4-aminopyridine (4-AP). The fish
195 were then placed in low melting agar and immersed in a solution of 4-AP (80 mM). Imaging
196 consisted of 5 minute intervals of the hindbrain or midbrain at a recording rate of 3 Hz. For each
197 indicator, 5 fish were imaged under 6 different field of views resulting in 834 and 1280 individual
198 cells for mNG-GECO1 and GCaMP6s, respectively (**Supplementary Fig. 6**). The resulting data
199 was evaluated using the Suite2p package (https://github.com/MouseLand/suite2p)[27]. We found
200 that mNG-GECO1 had a maximum $\Delta F/F_0$ for each cell of 3.09 ± 0.08 compared to 4.56 ± 0.11 for
201 GCaMP6s (**Fig. 3c**). The baseline fluorescence of GCaMP6s was higher compared to mNG-
202 GECO1 (0.95 ± 0.03 vs 1.41 ± 0.05 AU, respectively) (**Fig. 3d**). However, the signal-to-noise ratio
203 (SNR), which was computed by dividing the $\Delta F/F_0$ by the raw standard deviation of each cell in
204 six field of views, was higher for mNG-GECO1 (SNR = 6.63 ± 0.07) than GCaMP6s (SNR = 5.25
205 ± 0.04) (**Fig. 3e**). We also found that mNG-GECO1 had a slower decay time (faster k_{off} kinetics)
206 compared to GCaMP6s (1.98 ± 0.12 s^{-1} vs 3.00 ± 0.12 s^{-1}, respectively) (**Fig. 3f**). The overall data
207 in zebrafish neurons suggest that mNG-GECO1 is comparable in signal-to-noise ratio, kinetics,
208 and baseline brightness to the GCaMP6s sensor (**Supplementary Table 4**).

209 Ca^{2+} **imaging in human iPSC-derived cardiomyocytes**

210 Chemical Ca^{2+} dyes such as Fluo-4 acetoxymethyl (AM), Rhod-2 AM and Fura-2 AM are often
211 used to phenotype Ca^{2+} transients in induced pluripotent stem cell-derived cardiomyocytes (iSPC-
212 CM). However, these dyes can be toxic[28, 29] and may potentially suppress the activity of Na^+ and
213 K^+-dependent adenosine triphosphatase[30]. As such, we tested whether mNG-GECO1 could serve

214 as a robust tool for observing cells signaling and drug response while preventing cellular toxicity
215 in iPSC-CMs **(Supplementary Fig. 7).** We found that when iPSC-CMs expressing mNG-GECO1
216 o Fluo-4 AM were treated with 20 mM caffeine, mNG-GECO1 had a 2.8 fold higher ∆F/F response
217 than Fluo-4 (∆F/F = 11.77 ± 2.82 and 4.18 ± 1.27, respectively) **(Supplementary Fig. 7a, b).**
218 However, when cells were subjected to 0.33 Hz electrical stimulation for 30 minutes, mNG-
219 GECO1 had a slightly lower peak ∆F/F (2.26 ± 0.81) than Fluo-4 AM (3.31 ± 1.42)
220 **(Supplementary Fig. 7c, d).** We suspect that this discrepancy is due to mNG-GECO1s lower
221 affinity for Ca^{2+}. When we stimulated the cells in the presence of 20 mM caffeine, the max ∆F/F
222 of mNG-GECO1 (∆F/F = 14.20 ± 4.67) was higher than the max ∆F/F of Fluo-4 AM (∆F/F = 6.73
223 ± 1.19) **(Supplementary Fig. 7e, f).** Based on this data, we propose that mNG-GECO1 may serve
224 as a useful tool for phenotypic screening and functional tests in iPSC-CMs.

225

226 Conclusion

227 mNG-GECO1 is a new, first-generation, genetically encodable Ca^{2+} indicator that provides
228 performance comparable to 6th and 7th generation GCaMP indicators. We have demonstrated that
229 the *in vitro* performance of mNG-GECO1 in cultured HeLa cells is on par or better than GCaMP6s.
230 However, *in vitro* cultured neuron benchmarking as well as *in vivo* imaging in transgenic zebrafish
231 larvae have indicated that further directed evolution efforts will be required to produce an mNG-
232 GECO1 variant that provides substantial advantages relative to the jGCaMP7 series. Further
233 development of this indicator may come from increasing the Ca^{2+} affinity which would enable more
234 accurate single spike detection. In summary, we have developed a first generation GECI from the
235 mNG scaffold that retains the high fluorescent brightness *in vitro* with performance comparable
236 to the state-of-the-art GECI, GCaMP6s. We expect mNG-GECO1 to be just as amenable to
237 further optimization as the first generation GCaMP, and so mNG-GECO1 is likely to serve as the
238 parent of a new and improved lineage of high performance GECIs.

239 Author contributions

240 LZ, AA, and TP performed the directed evolution experiments and *in vitro* characterization. RP
241 performed the *in vitro* 2P characterization, IK and TGP conducted and analyzed the cultured
242 neuron experiments. RK conducted the initial expression experiments of mNG-GECO1 and its
243 variants in zebrafish under the supervision of WTA. VR completed the zebrafish characterization

under the supervision of MA. HYH and YFC did the experiments in human iPSC-derived cardiomyocytes. LZ, AA, KP, and REC wrote and edited the manuscript. All authors were allowed to review and edit the manuscript before publication.

Acknowledgments

We thank the University of Alberta Molecular Biology Services Unit (Alberta) and Molecular Bio (Janelia) for technical support. We thank Christopher Cairo (Alberta), Andy Holt (Alberta) and Loren Looger (Janelia) for providing access to the instrumentation, Eric Schreiter (Janelia) for providing access to resources and for useful feedback regarding the manuscript. We thank Deepika Walpia (Janelia) and the JRC Histology group for preparing cultured neurons. We thank John Macklin (Janelia) for overseeing two-photon measurements. We thank Nathan Shaner for the mNeonGreen fluorescent protein. REC acknowledges the Japan Society for the Promotion of Science (JSPS), Natural Sciences and Engineering Research Council of Canada (NSERC), and Canadian Institutes of Health Research (CIHR), for funding support. The mNG gene was a kind gift from Jiwu Wang at Allele Biotech.

References

1. Mank M, Griesbeck O. Genetically encoded calcium indicators. *Chem Rev* **108**, 1550-1564 (2008).
2. Akerboom J*, et al.* Optimization of a GCaMP Calcium Indicator for Neural Activity Imaging. *J Neurosci* **32**, 13819-13840 (2012).
3. Knopfel T. Genetically encoded optical indicators for the analysis of neuronal circuits. *Nat Rev Neurosci* **13**, 687-700 (2012).
4. Chen TW*, et al.* Ultrasensitive fluorescent proteins for imaging neuronal activity. *Nature* **499**, 295-300 (2013).
5. Pologruto TA, Yasuda R, Svoboda K. Monitoring neural activity and [Ca2+] with genetically encoded Ca2+ indicators. *J Neurosci* **24**, 9572-9579 (2004).
6. Tian L, Akerboom J, Schreiter ER, Looger LL. Neural activity imaging with genetically encoded calcium indicators. *Prog Brain Res* **196**, 79-94 (2012).
7. Deo C, Lavis LD. Synthetic and genetically encoded fluorescent neural activity indicators. *Curr Opin Neurobiol* **50**, 101-108 (2018).
8. Broussard GJ, Liang R, Tian L. Monitoring activity in neural circuits with genetically encoded indicators. *Front Mol Neuro* **7**, 1-17 (2014).
9. Kim TH*, et al.* Long-Term Optical Access to an Estimated One Million Neurons in the Live Mouse Cortex. *Cell Rep* **17**, 3385-3394 (2016).

10. Podor B, Hu YL, Ohkura M, Nakai J, Croll R, Fine A. Comparison of genetically encoded calcium indicators for monitoring action potentials in mammalian brain by two-photon excitation fluorescence microscopy. *Neurophotonics* **2**, 1-7 (2015).
11. Bootman MD, Allman S, Rietdorf K, Bultynck G. Deleterious effects of calcium indicators within cells; an inconvenient truth. *Cell Calcium* **73**, 82-87 (2018).
12. Steinmetz NA*, et al.* Aberrant Cortical Activity in Multiple GCaMP6-Expressing Transgenic Mouse Lines. *eNeuro* **4**, 1-15 (2017).
13. Helmchen F, Imoto K, Sakmann B. Ca2+ buffering and action potential-evoked Ca2+ signaling in dendrites of pyramidal neurons. *Biophys J* **70**, 1069-1081 (1996).
14. Ashworth R, Zimprich F, Bolsover SR. Buffering intracellular calcium disrupts motoneuron development in intact zebrafish embryos. *Dev Brain Res* **129**, 169-179 (2001).
15. Briston SJ, Dibb KM, Solaro RJ, Eisner DA, Trafford AW. Balanced changes in Ca buffering by SERCA and troponin contribute to Ca handling during β-adrenergic stimulation in cardiac myocytes. *Cardiovascular Res* **104**, 347-354 (2014).
16. Timofeeva Y, Volynski KE. Calmodulin as a major calcium buffer shaping vesicular release and short-term synaptic plasticity: facilitation through buffer dislocation. *Front Cell Neuro* **9**, 239-239 (2015).
17. Yang Y*, et al.* Improved calcium sensor GCaMP-X overcomes the calcium channel perturbations induced by the calmodulin in GCaMP. *Nat Commun* **9**, 1-18 (2018).
18. Barykina NV*, et al.* A new design for a green calcium indicator with a smaller size and a reduced number of calcium-binding sites. *Sci Rep* **6**, 1-15 (2016).
19. Barykina NV*, et al.* NTnC-like genetically encoded calcium indicator with a positive and enhanced response and fast kinetics. *Sci Rep* **8**, 1-19 (2018).
20. Dana H*, et al.* High-performance calcium sensors for imaging activity in neuronal populations and microcompartments. *Nat Methods* **16**, 649-657 (2019).
21. Shaner NC*, et al.* A bright monomeric green fluorescent protein derived from Branchiostoma lanceolatum. *Nat Methods* **10**, 407-409 (2013).
22. Wu J*, et al.* A long Stokes shift red fluorescent Ca2+ indicator protein for two-photon and ratiometric imaging. *Nat Commun* **5**, 1-11 (2014).
23. Clavel D*, et al.* Structural analysis of the bright monomeric yellow-green fluorescent protein mNeonGreen obtained by directed evolution. *Acta Crystallogr, Sect D* **72**, 1298-1307 (2016).
24. Ai H-w, Baird MA, Shen Y, Davidson MW, Campbell RE. Engineering and characterizing monomeric fluorescent proteins for live-cell imaging applications. *Nat Protoc* **9**, 910-928 (2014).
25. Palmer AE, Tsien RY. Measuring calcium signaling using genetically targetable fluorescent indicators. *Nat Protoc* **1**, 1057-1065 (2006).
26. Kawakami K, Takeda H, Kawakami N, Kobayashi M, Matsuda N, Mishina M. A Transposon-Mediated Gene Trap Approach Identifies Developmentally Regulated Genes in Zebrafish. *Dev Cell* **7**, 133-144 (2004).
27. Pachitariu M*, et al.* Suite2p: beyond 10,000 neurons with standard two-photon microscopy. *bioRxiv*, 1-30 (2017).
28. Shinnawi R*, et al.* Monitoring Human-Induced Pluripotent Stem Cell-Derived Cardiomyocytes with Genetically Encoded Calcium and Voltage Fluorescent Reporters. *Stem Cell Reports* **5**, 582-596 (2015).
29. Chang Y-F*, et al.* Non-invasive phenotyping and drug testing in single cardiomyocytes or beta-cells by calcium imaging and optogenetics. *PLOS ONE* **12**, 1-17 (2017).
30. Smith NA, Kress BT, Lu Y, Chandler-Militello D, Benraiss A, Nedergaard M. Fluorescent Ca2+ indicators directly inhibit the Na,K-ATPase and disrupt cellular functions. *Science Signaling* **11**, 1-14 (2018).

326 31. Cranfill PJ*, et al.* Quantitative assessment of fluorescent proteins. *Nat Methods* **13**, 557-562
327 (2016).
328 32. Tsien R, Pozzan T. [14] Measurement of cytosolic free Ca2+ with quin2. In: *Methods Enzymol*).
329 Academic Press (1989).
330 33. Dweck D, Reyes-Alfonso A, Potter JD. Expanding the range of free calcium regulation in
331 biological solutions. *Anal Biochem* **347**, 303-315 (2005).
332 34. Xu C, Webb WW. Measurement of two-photon excitation cross sections of molecular
333 fluorophores with data from 690 to 1050 nm. *J Opt Soc Am B: Opt Phys* **13**, 481-491 (1996).
334 35. Mütze J*, et al.* Excitation Spectra and Brightness Optimization of Two-Photon Excited Probes.
335 *Biophysical Journal* **102**, 934-944 (2012).
336 36. Palmer AE, Tsien RY. Measuring calcium signaling using genetically targetable fluorescent
337 indicators. *Nat Protoc* **1**, 1057-1065 (2006).
338 37. Wardill TJ*, et al.* A Neuron-Based Screening Platform for Optimizing Genetically-Encoded
339 Calcium Indicators. *PLOS ONE* **8**, e77728 (2013).
340 38. Thorn RJ, Clift DE, Ojo O, Colwill RM, Creton R. The loss and recovery of vertebrate vision
341 examined in microplates. *PLOS ONE* **12**, 1-17 (2017).

342

343 # Methods

344 ## General procedures

345 Synthetic DNA oligonucleotides and gBlocks were purchased from Integrated DNA Technologies.
346 Plastic consumables, restriction endonucleases, Taq polymerase, Phusion polymerase, T4 DNA
347 ligase, deoxynucleotides, DH10B *E. coli*, pBAD/His B plasmid, pcDNA3.1(+) plasmid, Bacterial
348 Protein Extraction Reagent (B-PER), Penicillin-Streptomycin, Fetal Bovine Serum (FBS),
349 TurboFect, Lipofectamine 2000, and GeneJet gel or plasmid purification kits were purchased from
350 Thermo Scientific. Endotoxin-free plasmid DNA isolation kits were purchased from Qiagen (cat.
351 12362). Agarose, $MnCl_2 \cdot 4H_2O$, tryptone, D-glucose, ampicillin, L-arabinose, Hank's balanced salt
352 solution (HBSS), DMEM, TrypLE Express, and LB Lennox media were purchased from Fisher
353 Scientific. NbActiv4 and neuron transfection media were purchased from Brain Bits.

354 3-(N-morpholino)propanesulfonic acid (MOPS), ethylene glycol-bis(2-aminoethylether)-
355 N,N,N′,N′-tetraacetic acid (EGTA), and nitrilotriacetic acid (NTA), were purchased from VWR.
356 Nickel NTA immobilized metal affinity chromatography protein purification beads were purchased
357 from G-BioSciences. Ionomycin and tricaine methanesulfonate were purchased from Millipore-
358 Sigma. Ethidium bromide and PCR machines (T100 Thermal Cycler) were purchased from
359 BioRad. Gibson Assembly reagent was purchased from New England Biolabs (NEB). Genemorph
360 II Random Mutagenesis kits and QuikChange mutagenesis kits were purchased from Agilent
361 Technologies. Nunc 96-Well Polypropylene DeepWell Storage Plates (cat. 278743) and 96-well
362 Nunc MicroWell 96-Well Optical-Bottom Plates (cat. 265301) were purchased from Thermo
363 Scientific. Molecular weight cut off filters were purchased from Millipore-Sigma. Sequencing was
364 completed by the Molecular Biology Services Unit at the University of Alberta.

365 ## Molecular biology and protein engineering

366 Libraries for iterative directed evolution were created using Genemorph II Random Mutagenesis
367 kits and NEB's Gibson Assembly reagent. Blunt ended linear DNA fragments with random
368 mutations are created using the Genemorph II kit according to the manufacturer's
369 recommendations. Genemorph II PCR product was ligated using NEB Gibson Assembly reagent
370 into a linearized pBAD vector cut with XhoI/HindIII. Site saturation mutagenesis libraries were
371 created using single and multi QuikChange mutagenesis kits according the manufacturers
372 recommendations.

373 Libraries are transformed into DH10B *E. coli* and plated on 100 µg/L ampicillin/1.5% agar plates
374 with 0.02% L-arabinose and grown overnight (12-18 hours) at 37 °C. Colonies are selected on
375 the basis of fluorescence intensity, picked, and placed into 96 DeepWell blocks containing 1.3 mL
376 of LB Lennox media supplemented with 100 µg/mL ampicillin and 0.02% L-arabinose. Deepwell
377 blocks were shaken overnight at 37 °C. The next day, blocks are centrifuged at 6000 × g for 5
378 minutes to pellet cells. Media was discarded and 30 µL of B-PER was added to each well. After
379 shaking for 15 minutes, 200 µL of 10 mM EGTA in 30 mM MOPS/100 mM KCl pH 7.2 (MOPS/KCl
380 buffer) is added to each well of the blocks before mixing briefly and being centrifuged again for 5
381 minutes at 6000 × g. 90 µL of the resulting lysate is loaded in each well of 96-well optical bottom
382 plates. Fluorescence intensity for each well of the plate is then read with a Tecan Safire[2]
383 microplate reader to determine the low Ca^{2+} intensity for each variant. High Ca^{2+} intensity is
384 acquired by adding 15 µL of 100 mM Ca^{2+} in 30 mM MOPS pH 7.2 with a 60 second shake before
385 reading. Taking the value of the high Ca^{2+} intensity divided by the low Ca^{2+} intensity gives a
386 relative sensitivity value. Promising candidates, usually 10% of each 96-well block, are retested
387 from the lysate in 10 mM low (EGTA chelated) and 10 mM high Ca^{2+} solution diluted in MOPS/KCl
388 buffer. The plasmids associated with the promising variants are sent for sequencing and used as
389 template for the next round of directed evolution. For cultured neuron field stimulation
390 experiments, GCaMP6s, jGCaMP7f, jGCaMP7s, jGCaMP7c, and jGCaMP7b plasmids (available
391 on Addgene) were subcloned into a syn-<*GCaMP*>-IRES-mCherry-WPRE-pA vector.

392 Constructs for zebrafish transfection were created by ligating mNG-GECO1 PCR product into a
393 Tol2 transposon backbone. Briefly, PCR of mNG-GECO variants were ligated into Tol2-HuC-H2B
394 vector (Addgene plasmid #59530) cut with SalI/AgeI using Gibson Assembly. The ligated
395 constructs were transformed into NEB Turbo Competent *E. coli* cells and grown in 250 µL culture
396 overnight at 30 °C. The next day, the culture is pelleted, and the DNA is purified using endotoxin-
397 free plasmid DNA purification protocol using EndoFree Plasmid Maxi Kit. The DNA is eluted with
398 EF-free H_2O and verified by sequencing.

399 **Protein purification and *in vitro* characterization**

400 To purify mNG, mNG-GECO variants, and GCaMP6s for *in vitro* characterization, pBAD/His B
401 plasmid containing the gene of interest was used to transform electrocompetent DH10B *E. coli*,
402 which were then streaked on 100 µg/mL ampicillin/1.5% agar plates. After overnight incubation at
403 37 °C, a single colony was picked and inoculated to a 2 L flask containing 500 mL of 100 µg/mL
404 ampicillin/0.02% L-arabinose liquid media and cultured for 24-30 hours at 37 °C. The culture is

405 then centrifuged at 6000 × g for 6 minutes to collect the cells. Cells are re-suspended in 30 mL of
406 cold Tris buffered saline (TBS, 150 mM NaCl, 50 mM Tris-HCl) pH 8.0 and lysed by sonication
407 (QSonica Q700, amplitude 50, 1 second on, 2 seconds off, 3 minutes sonication time). All
408 subsequent purification procedures were performed on ice. The resulting lysate was clarified of
409 cell debris by centrifugation for 1 hour at 21,000 × g, filtered through a Kim-wipe into a 50 mL
410 conical bottom tube, and incubated for 3 hours with Ni-NTA resin. Resin containing NTA bound
411 protein was washed with 100 mL of 20 mM imidazole TBS wash buffer and eluted with 250 mM
412 imidazole TBS elution buffer. Purified protein was buffer exchanged into TBS using a 10,000 Da
413 molecular weight cut-off filter (Millipore-Sigma) through 3 successive washes. Absorption spectra
414 were recorded on a Beckman-Coulter DU-800 UV-visible spectrophotometer and fluorescence
415 spectra recorded on a Tecan Safire[2] plate reader.

416 Extinction coefficient determination for mNG-GECO variants were performed using the alkaline
417 denaturation method with mNG as a standard[31]. Briefly, the concentration of protein was adjusted
418 by dilution in MOPS/KCl pH 7.2 to reach an absorbance of 0.6 to 1.0. A dilution series with
419 MOPS/KCl and 10 mM Ca^{2+} was then prepared with absorbances of 0.01, 0.02, 0.03, 0.04, and
420 0.05 for mNG, mNG-GECO variants, and GCaMP6s. Integration of the fluorescent peaks provides
421 a total fluorescent emission value which was plotted against the absorbance to provide a slope.
422 The quantum yields of mNG-GECO variants were determined using the published[31] QY value of
423 mNG in a ratiometric manner:

424 $$\Phi_{protein} = \Phi_{standard} \times (S_{protein}/S_{standard})$$

425 Extinction coefficients were determined by measuring the absorption spectrum in MOPS/KCl pH
426 7.2 and 2 M NaOH. The absorbance value for the denatured GFP peak at 440 nm was divided
427 by the previously determined extinction coefficient of 44,000 $M^{-1}cm^{-1}$ to give the concentration of
428 protein[31]. Using Beer's law, the extinction coefficient was then determined by dividing the TBS
429 sample absorbance maximum by the calculated protein concentration.

430 Determination of K_d was performed as previously described[32, 33]. Briefly, a reciprocal dilution series
431 was created with either 10 mM EGTA/10 mM Ca^{2+} EGTA ranging in free Ca^{2+} concentration of 0
432 to 0.039 mM or 10 mM NTA/10 mM Ca^{2+} NTA ranging in free Ca^{2+} concentration from 0 to 1.13
433 mM[33]. An equal amount of purified mNG-GECO was diluted 100× into 100 µL of buffer and the
434 intensity plotted against free Ca^{2+} in triplicate. The data are then fit to a four-parameter variable-
435 slope in GraphPad Prism 7 software to determine the K_d.

436 **Two Photon Measurements**

437 The two photon measurements were performed in 39 μM free Ca^{2+} (+Ca^{2+}) buffer (30 mM MOPS,
438 10 mM CaEGTA in 100 mM KCl, pH 7.2) or 0 μM free Ca^{2+} (-Ca^{2+}) buffer (30 mM MOPS, 10 mM
439 EGTA in 100 mM KCl, pH 7.2). The two photon excitation spectra were acquired as previously
440 described[2]. Protein solution of 2 – 4 μM concentration in +Ca^{2+} or -Ca^{2+} buffer was prepared and
441 measured using an inverted microscope (IX81, Olympus) equipped with a 60×, 1.2 NA water
442 immersion objective (Olympus). Two photon excitation was obtained using an 80 MHz Ti-
443 Sapphire laser (Chameleon Ultra II, Coherent) for spectra from 710 nm to 1080 nm. Fluorescence
444 collected by the objective was passed through a short pass filter (720SP, Semrock) and a band
445 pass filter (550BP200, Semrock), and detected by a fiber-coupled Avalanche Photodiode (APD)
446 (SPCM_AQRH-14, Perkin Elmer). The obtained two photon excitation spectra were normalized
447 for 1 μM concentration and further used to obtain the action cross-section spectra (AXS) with
448 fluorescein as a reference[34].

449 Fluorescence correlation spectroscopy (FCS) was used to obtain the 2P molecular brightness of
450 the protein molecule. The molecular brightness was defined by the rate of fluorescence obtained
451 per total number of emitting molecules. 50-200 nM protein solutions were prepared in +Ca^{2+} buffer
452 and excited with 940 nm wavelength at various power ranging from 2-30 mW for 200 seconds.
453 The obtained fluorescence was collected by an APD and fed to an autocorrelator (Flex03LQ,
454 Correlator.com). The obtained autocorrelation curve was fit on a diffusion model through an inbuilt
455 Matlab function[35] to determine the number of molecules <N> present in the focal volume. The 2-
456 photon molecular brightness (ε) at each laser power was calculated as the average rate of
457 fluorescence $\langle F \rangle$ per emitting molecule $\langle N \rangle$, defined as $\varepsilon = \langle F \rangle / \langle N \rangle$ in kilocounts per second
458 per molecule (kcpsm). As a function of laser power, the molecular brightness initially increases
459 with increasing laser power, then levels off and decreases due to photobleaching or saturation of
460 the protein chromophore in the excitation volume. The maximum or peak brightness achieved,
461 $\langle \varepsilon_{max} \rangle$, represents a proxy for the photostability of a fluorophore.

462 ***In vitro* kinetics analysis by stopped-flow**

463 Rapid kinetic measurements of purified mNG-GECO1 and GCaMP6s were made using an
464 Applied Photophysics SX-20 Stopped-flow Reaction Analyzer exciting at 488 nm with 2 nm
465 bandwidth and collecting light at 520 nm through a 10 mm path at room temperature. Briefly, 2
466 μM of mNG-GECO1 and GCaMP6s proteins in 1 mM Ca^{2+} (30 mM MOPS, 100 mM KCl, pH 7.2)
467 were rapidly mixed at 1:1 ratio with 50 mM of EGTA (same buffer as above) at room temperature.

468 k_{off} values were determined by fitting a single exponential dissociation curve to the signal decay
469 using Graphpad Prism, with units of s^{-1}. For k_{on}, both proteins buffered in 30 mM MOPS, 100 mM
470 KCl, 50 μM EGTA were rapidly mixed at 1:1 ratio with varying concentrations of Ca^{2+} produced
471 by reciprocal dilutions of 10 mM EGTA and 10 mM CaEGTA. The measured fluorescence change
472 overtime was fitted using a 2-phase association curve to obtain the slow and fast observed rate
473 constants (k_{obs}) for each free Ca^{2+} concentration. All measurements were done in triplicates, and
474 values are reported as mean ± s.e.m. where noted.

475 **Fluorescence live cell imaging**

476 **Imaging in HeLa cells.** We followed previously reported protocols for our Ca^{2+} imaging
477 experiments[36]. Briefly, HeLa cells cultured in DMEM with 10% fetal bovine serum supplemented
478 with penicillin-G potassium salt (50 units/mL) and streptomycin sulphate (50 μg/mL) were plated
479 on collagen coated 35 mm glass bottom dishes. HeLa cells are transfected at 60% confluency
480 with 1 μg of pcDNA3.1(+) harboring the variant of interest using 2 μL of TurboFect according to
481 the manufacturer's recommendation. After overnight incubation at 37 °C with 5% CO_2, cells were
482 washed twice with prewarmed Hank's balanced salt solution immediately before imaging.

483 Imaging of transfected HeLa cells was performed on an inverted Zeiss 200M microscope with
484 Semrock filters (excitation 470/40, emission 525/50) and captured with an OrcaFlash 4.0 –
485 C13440 (Hamamatsu). Images were acquired through a 40× (N.A. 1.3) oil immersion lens using
486 MetaMorph 7.8.0.0 software and an MS-2000 automated stage (Applied Scientific
487 Instrumentation).

488 **Imaging in dissociated rat cortical neurons.**

489 The mNG-GECO1 indicator was compared to other GECIs in a field stimulation assay[37]. Neonatal
490 (P0) rat pups were euthanized, and their cortices were dissected and dissociated using papain
491 (Worthington). Cells were transfected by combining $5x10^5$ viable cells with 400 ng plasmid DNA
492 and nucleofection solution electroporation cuvettes (Lonza). Electroporation was performed
493 according to the manufacturer instructions. Cells were then plated at a density of $5x10^5$ cells/well
494 in poly-D-lysine (PDL) coated 96-well plates. After 14-18 days in vitro, culture medium was
495 exchanged for an imaging buffer solution with a drug cocktail to inhibit synaptic transmission[37].
496 The field stimulation assay was performed as previously described[4, 20, 37]. Briefly, neurons were
497 field stimulated (1, 2, 3, 5, 10, 20, 40, 160 pulses at 83 Hz, 1 ms, 40V), and concurrently imaged
498 with an electron multiplying charge coupled device (EMCCD) camera (Andor iXon DU897-BV,

499 198 Hz, 4x4 binning, 800 x 800 μm, 1,400 frames). Reference images were taken after stimulation
500 to perform cell segmentation during analysis. Illumination was delivered by blue light (470 nm,
501 Cairn Research Ltd; excitation: 450-490 nm; emission: 500-550 nm; dichroic: 495 nm long-pass).
502 The illumination power density was measured to be 19 mW/mm^2 at the sample. Stimulation pulses
503 were synchronized with the camera using data acquisition cards (National Instruments), controlled
504 with Wavesurfer software (https://wavesurfer.janelia.org/). Imaging was performed at room
505 temperature. Data were analyzed using previously-developed MATLAB (Mathworks) scripts[20, 37].

506 Ca^{2+} **imaging in human iPSC-derived cardiomyocytes**

507 Human iPSC-derived cardiomyocytes (human iPSC Cardiomyocytes - male | ax2505) were
508 purchased from Axol Bioscience. The 96 well glass-bottom plate or MatTek glass bottom dish
509 (Ashland, MA, US) were first coated with Fibronectin/Gelatin (0.5% / 0.1%) at 37 °C for at least 1
510 hour. The cells were plated and cultured for three days in Axol's Cardiomyocyte Maintenance
511 Medium. The cells then were ready for final observation with Tyrode's buffer. For electrical
512 stimulations, iPSC derived cardiomyocytes were plated on MatTek glass bottom dish (Ashland,
513 MA, US) at 100,000 cells/well. Electrical stimulation was done with 10 V, 10 ms duration and 3
514 seconds internal using myopacer (Ion optix c-pace ep). To image, an inverted microscope (DMi8,
515 Leica) equipped with a 63× objective lens (NA 1.4) and a multiwavelength LED light source (pE-
516 4000, CoolLED) was used. iPSC derived cardiomyocytes were plated out as above, and then
517 loaded with 5 μM Fluo-4-AM (Thermo-Fisher, UK) at room temperature for 10 minutes, free dye
518 was washed off by media replacement with pre-heated culture media, followed by imaging with
519 iXon EMCCD (Andor) camera using 488 nm LED illumination. The GFP filter set (DS/FF02-
520 485/20-25, T495lpxr dichroic mirror, and ET525/50 emission filter) was used for Fluo-4 and mNG-
521 GECO1 observation.

522 **Imaging of zebrafish larvae.**

523 To demonstrate the sensitivity and brightness of mNG-GECO1 *in vivo*, we performed
524 fluorescence imaging of Ca^{2+} activity in a subset of neurons in larval zebrafish. Initially, we used
525 the AB/WIK zebrafish strain for morphology studies (**Supplementary Fig. 4)**, which were treated
526 with 1-phenol-2-thiourea (PTU) to inhibit pigmentation, as described previously[38]. Later, *Casper*
527 strains were available and 20 ng/μL DNA plasmids encoding mNG-GECO1 under the control of
528 nuclear-localized elavl3/HuC promoter (Addgene: 59530) were injected into two-cell stage
529 embryos of *Casper* mutant zebrafish[33] with 40 ng/μl Tol2 transposase mRNA (26) to generate F0
530 transgenic zebrafish. Imaging experiments were performed using 6 day old embryos. Embryos

531 showing expression were treated with 1 mg/mL bath-applied α-bungarotoxin (Thermo Fischer
532 Scientific, B1601) dissolved in external solution for 30 seconds to block movement, and
533 subsequently incubated with 80 mM 4-aminopyridine (4AP) for 10 minutes. After incubation, the
534 larvae were embedded in 2% low melting temperature agarose to prevent motion. For earlier
535 imaging (**Supplementary Fig. 4)** a Zeiss 700 confocal microscope was used with A-Plan 10x/0.25
536 Ph1 M27 objective lens to obtain picture from the whole larvae (**Supplementary Fig. 4a**). For
537 enlarged areas (**Supplementary Fig. 4b-e**), a Plan-Apochromat 20x/0.8 M27 lens was used.
538 Later imaging was performed using a 488 nm laser (0.45 μM) and a 525/50 nm emission filter at
539 3 Hz using Zeiss 880 confocal microscope. The laser power was set to 2.3%, gain 720, and
540 pinhole to 29.3% open. Image acquisition, data registration, segmentation and cell traces were
541 handled using theSuite2p package in Python. All animal procedures were approved by the
542 Institutional Animal Care and Use Committee at the HHMI Janelia Research Campus or by the
543 Animal Care and Use Committee: Biosciences at the University of Alberta.

544 **Figures and Supplementary Data**

545

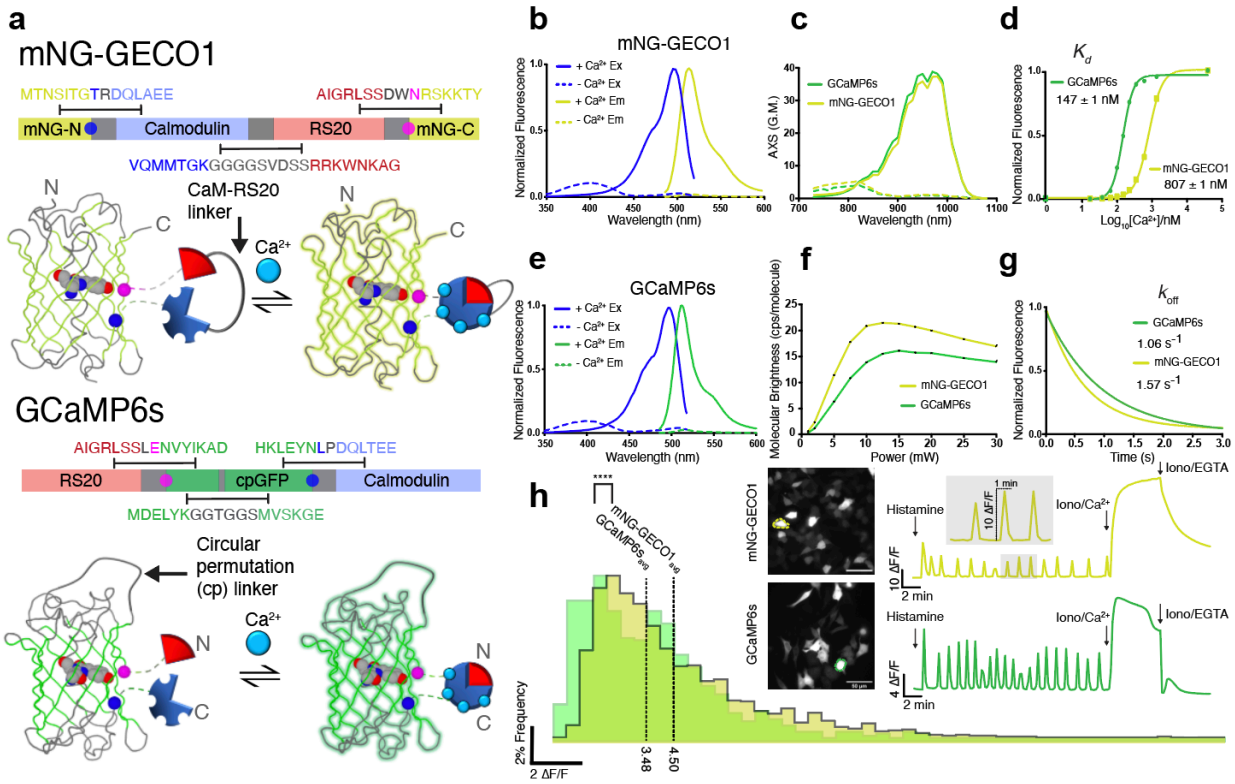

546

547 **Figure 1 Topology and *in vitro* characterization of mNG-GECO1 and GCaMP6s**

548 **a** Topology of non-circularly permuted mNG-GECO1 and circularly permuted GCaMP6s. Linker
549 regions are shown in grey and the two residues that flank the insertion site (residue 136 of mNG
550 in blue and residue 139 in magenta; numbering as in PDB ID 5LTR)[23] are shown as circles on
551 both the protein structure and gene schematics. The Ca^{2+} responsive domains are shaded light
552 blue for CaM and light red for RS20. **b**,**e** Excitation and emission spectra for each indicator. **c** 2-
553 photon cross section for each indicator in Ca^{2+} saturated or Ca^{2+} free states. **d** Ca^{2+} titration for
554 GCaMP6s (K_d = 147 ± 1 nM) and mNG-GECO1 (807 ± 1 nM). **f** Dependence of two-photon
555 molecular brightness on excitation power intervals. **g** Stop-flow kinetics for each indicator showing
556 mNG-GECO1 (k_{off} 1.57 s^{-1}) and GCaMP6s (k_{off} 1.06 s^{-1}). **h** Characterization of histamine induced
557 Ca^{2+} oscillations in HeLa cells with representative traces inset.

558

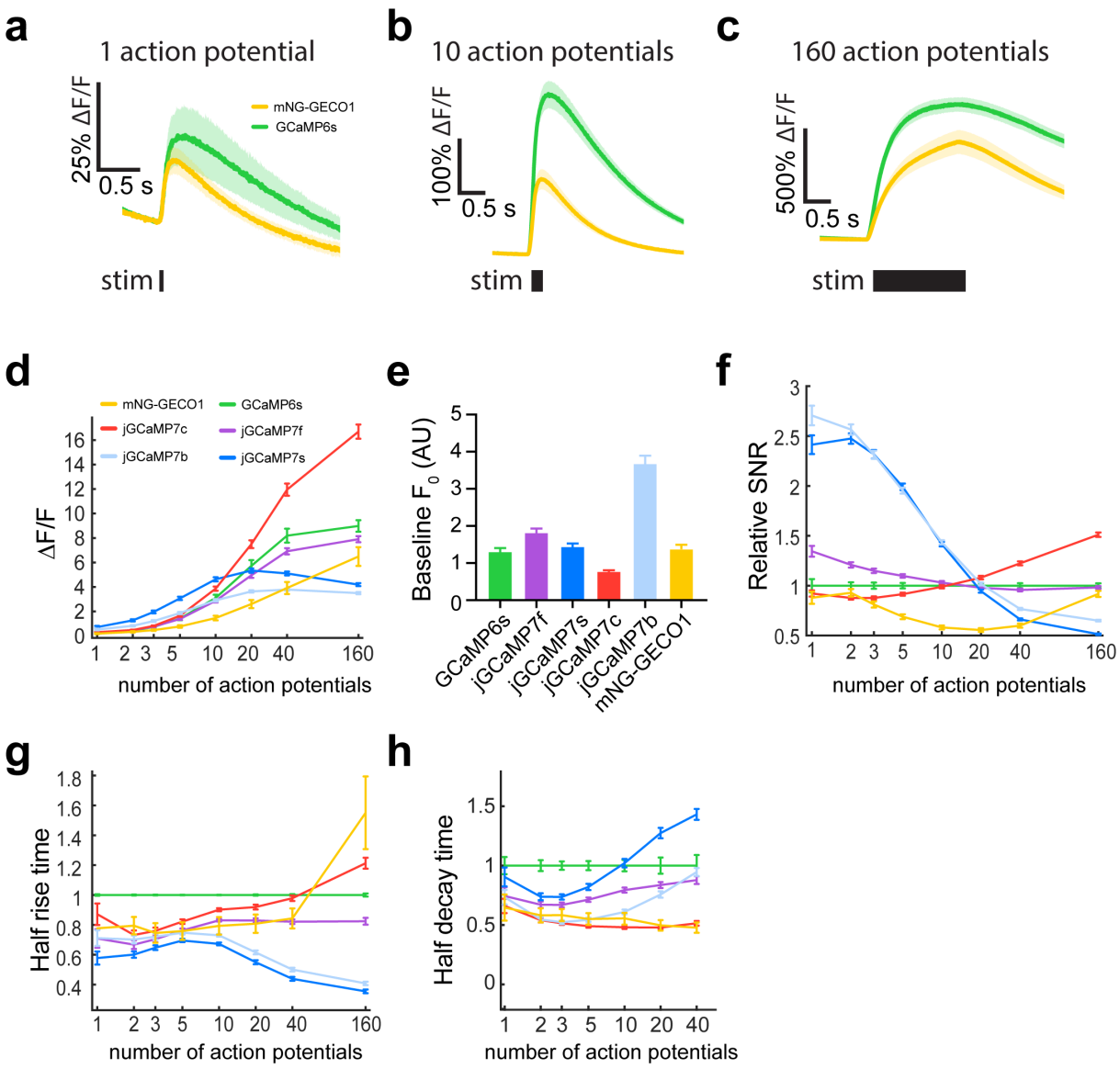

Figure 2 Characterization of mNG-GECO1 and GCaMP series indicators in dissociated rat hippocampal neurons

a-c Average responses to 1, 10, and 160 action potentials for mNG-GECO1 and GCaMP6s. Shaded areas correspond to s.e.m. for each trace. **d** Response amplitude $\Delta F/F_0$ for mNG-GECO1 and the GCaMP series of indicators in response to 1, 2, 3, 5, 10, 20, 40, and 160 action potentials. Data are presented normalized to $\Delta F/F_0$ of GCaMP6s. **e** Baseline brightness for each indicator, defined as the mean raw fluorescence intensity of all neurons prior to the stimulus. **f** Relative SNR, defined as the peak raw fluorescence divided by the signal standard deviation prior to the stimulus, normalized to SNR of GCaMP6s. **g** Half-rise time normalized to GCaMP6s. **h** Half-decay

time normalized to GCaMP6s. The 160 action potential measurement was omitted because fluorescence levels generally did not return to baseline over the imaging period. For **a**-**h**, mNG-GECO1: 621 neurons, 15 wells; GCaMP6s: 937 neurons, 17 wells; jGCaMP7c: 2,551 neurons, 44 wells; jGCaMP7b: 2,339 neurons, 47 wells; jGCaMP7f: 2,585 neurons, 48 wells; and jGCaMP7s: 2,249 neurons, 47 wells. Data in **d**-**h** shown as mean ± s.e.m., see **Supplementary Table 3** for analyzed data.

576

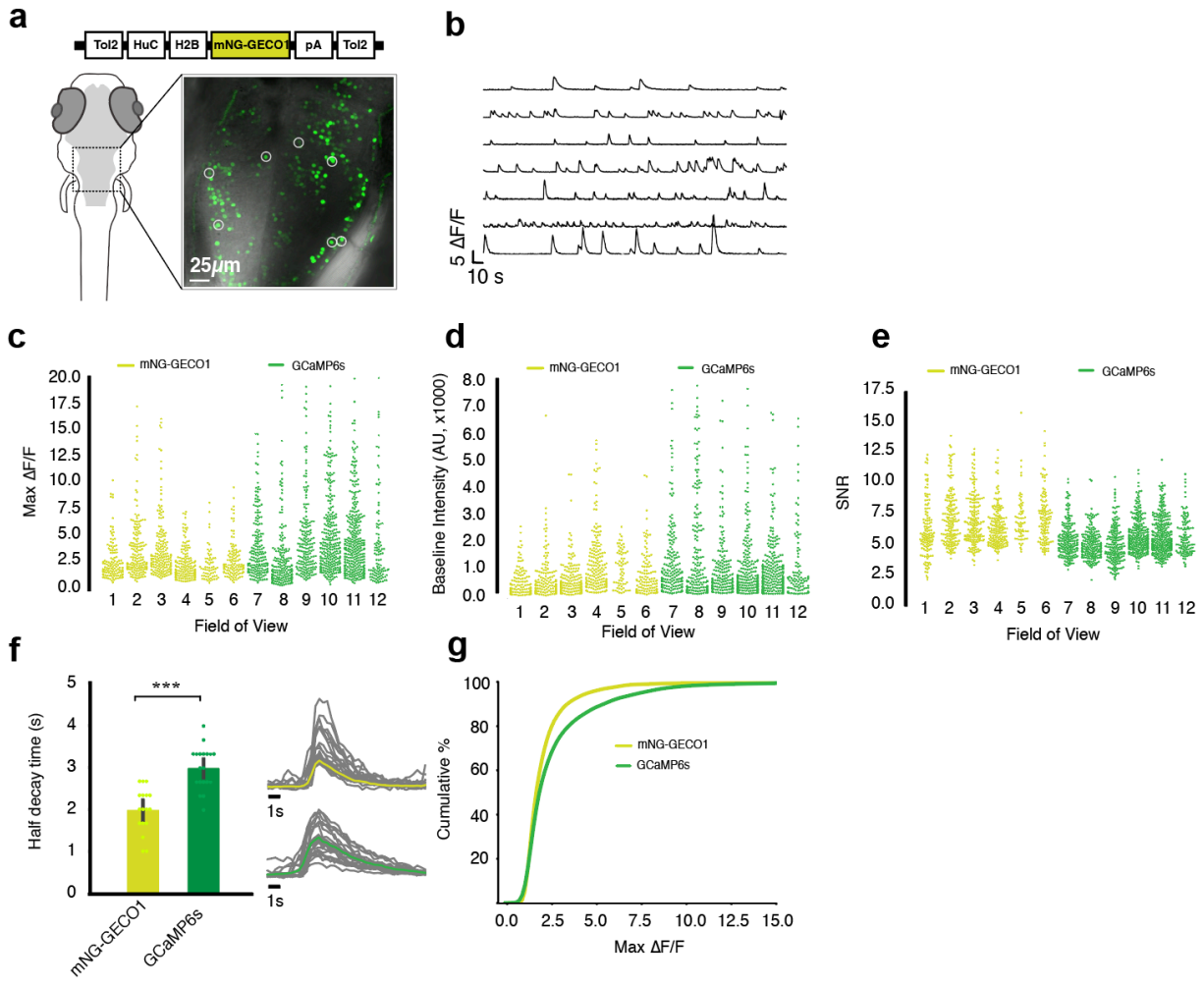

577

578 **Figure 3 Characterization of mNG-GECO1 and GCaMP6s in transgenic zebrafish hind brain**
579 **tissue.** **a** Schematic representation of Tol2[HuC-H2B-mNG-GECO1] construct and confocal
580 image of one fish (5 to 6 days post fertilization) with 7 region of interests (ROI) circled. **b** Traces
581 of ROI's from a). **c** Max $\Delta F/F_0$ calculated by taking the max peak of each cell within the field of
582 interest over 5 minutes; six ROI's each are used from 5 independent fish expressing mNG-
583 GECO1 and 5 fish expressing GCaMP6s. **d** Baseline fluorescence intensity of each cell within all
584 ROI's from 5 fish; confocal settings are kept consistent between GCaMP6s and mNG-GECO1
585 imaging. **e** Signal-to-noise ratio (SNR) computed by dividing $\Delta F/F_0$ by raw standard deviation of
586 each cell across 6 FOV's each for both sensors. **f** Average half decay time plotted for mNG-
587 GECO1 (n = 17) and GCaMP6s (n = 19) by averaging randomly selected peaks. **g** Cumulative

distribution of mNG-GECO1 vs. GCaMP6s. All cells are arranged in incremental order of $\Delta F/F_0$ and plotted with respect to their $\Delta F/F_0$ and their position in the order (%).

590 **Supplementary Figures and Tables**

591 **Supplementary Table 1. In vitro characterization of mNG-GECO1 and GCaMP6s.** mNG,
592 mNG-GECO1, and GCaMP6s were purified and tested in parallel. mNG was used as a standard
593 for brightness and quantum yield determination.

Indicator	Excitation Max (nm) (Ca^{2+} sat.)	Emission Max (nm) (Ca^{2+} sat.)	Quantum Yield (Ca^{2+} sat.)	Extinction Coefficient ($mM^{-1}cm^{-1}$; Ca^{2+} sat.)	Brightness[a]	Brightness Relative to GCaMP6s	Brightness Relative to mNG	$\Delta F/F_0$	K_d (nM)	k_{off} (s^{-1})
mNeonGreen	506	517	0.8[b]	112,000 +/- 900	90	205%	100%	NA	NA	NA
mNG-GECO1	496	513	0.69 +/- 0.01	102,000 +/- 2,700	70	159%	78%	35	807 +/- 1	1.57 +/- 0.01
GCaMP6s	497	512	0.59 +/- 0.02	74,000 +/- 500	44	100%	49%	39	147 +/- 1	1.06 +/- 0.01

[a]Product of ε in $mM^{-1}cm^{-1}$ and Φ (no units)

[b]From Ref.[21]

594

595 **Supplementary Table 2. Characterization of Ca^{2+}-dependent fluorescence of mNG-GECO1**
596 **and GCaMP6s in HeLa cells**. Cells were treated with histamine (abb. His), then with
597 Ca^{2+}/ionomycin (abb. Ca^{2+}), and then with EGTA/ionomycin (abb. EGTA). n is the total number of
598 cells recorded over five independent transfections. The oscillations were detected in all cells with
599 a prominence of greater than 0.5 using a Matlab script. Errors are s.d.

Protein	Number of HeLa cells (n)	Total Number of oscillations detected	Maximum Ca^{2+} to minimum EGTA $\Delta F/F_0$	Maximum His to minimum His ratio	Maximum His to maximum Ca^{2+} ratio
mNG-GECO1	137	1624	4.50 ± 2.96	48.8 ± 15.1	16.8 ± 10.5
GCaMP6s	99	687	3.48 ± 2.40	16.7 ± 5.2	12.8 ± 6.11

600

601 **Supplementary Table 3. mNG-GECO1 comparison with GCaMP series sensors in**
602 **dissociated rat hippocampal neurons**. Median values were calculated per well and mean (of
603 medians) ± s.e.m. are presented. SNR values were calculated per individual cells, and median ±
604 s.e.m are shown.

Protein	1 AP $\Delta F/F_0$ amplitude	3 AP $\Delta F/F_0$ amplitude	10 AP $\Delta F/F_0$ amplitude	160 AP $\Delta F/F_0$ amplitude	Baseline Brightness (Fluorescence Intensity (AU))	Half rise time 3 APs (ms)	Half decay time 3 APs (ms)	SNR 1 APs	SNR 3 APs
mNG-GECO1	0.19±0.04	0.5±0.07	1.5±0.19	6.5±0.8	1374±31	49±1	582±12	8.9±0.01	20.3±0.02
GCaMP6s	0.27±0.09	0.7±0.08	3.1±0.26	9.0±0.47	1302±26	65±2	1,000±36	10.1±0.07	25.0±0.03
jGCaMP7b	0.6±0.07	1.2±0.08	2.9±0.1	3.5±0.09	3673±32	47±0.1	523±2	27.4±0.01	57.8±0.01
jGCaMP7c	0.3±0.03	0.8±0.04	3.9±0.2	16.7±0.58	770±6	49±0.1	513±1	9.3±0.003	21.9±0.01
jGCaMP7f	0.3±0.06	0.8±0.05	2.9±0.1	7.9±0.25	1797±16	46±0.1	669±2	13.6±0.01	28.7±0.01
jGCaMP7s	0.7±0.10	2.0±0.11	4.6±0.17	4.2±0.12	1397±11	42±0.1	736±2	24.5±0.01	57.9±0.02

605

606

607 **Supplementary Table 4. mNG-GECO1 comparison with GCaMP6s in larval zebrafish 6 dpf**.
608 Mean values were calculated for the total number of cells (ROI's) across six FOV's in five
609 independent fish. Mean ± s.e.m. are presented. For max $\Delta F/F_0$, the maximum $\Delta F/F_0$ from each
610 cell is used. For baseline brightness, the raw intensity of the indicator under the same set of
611 imaging conditions is used. For half decay time, 17 and 19 represented cells were used for mNG-
612 GECO1 and GCaMP6s, respectively. The difference in max $\Delta F/F_0$ for the two indicators is
613 significant (Kolmogorov-Smirnov statistic = 0.218, p-value = 1.79×10^{-21}). The difference in
614 baseline brightness for the two indicators is significant (Kolmogorov-Smirnov statistic = 0.100, p-
615 value ≈ 7.31×10^{-5}). The difference in half decay time for the two indicators is significant
616 (Kolmogorov-Smirnov statistic = 0.666, p-value ≈ 3.00×10^{-4}).

Protein	**# of biological replicates**	**# of total field of views (FOV)**	**# of total cells (N)**	**Max $\Delta F/F_0$**	**Baseline Brightness (×1000) (AU)**	**Signal to noise ratio (SNR)**	**Half decay time (s^{-1}) (n)**
mNG-GECO1	5	6	834	3.09 ± 0.08	0.95 ± 0.03	6.63 ± 0.07	1.98 ± 0.12 (17)
GCaMP6s	5	6	1280	4.56 ± 0.11	1.41 ± 0.05	5.25 ± 0.04	3.00 ± 0.12 (19)

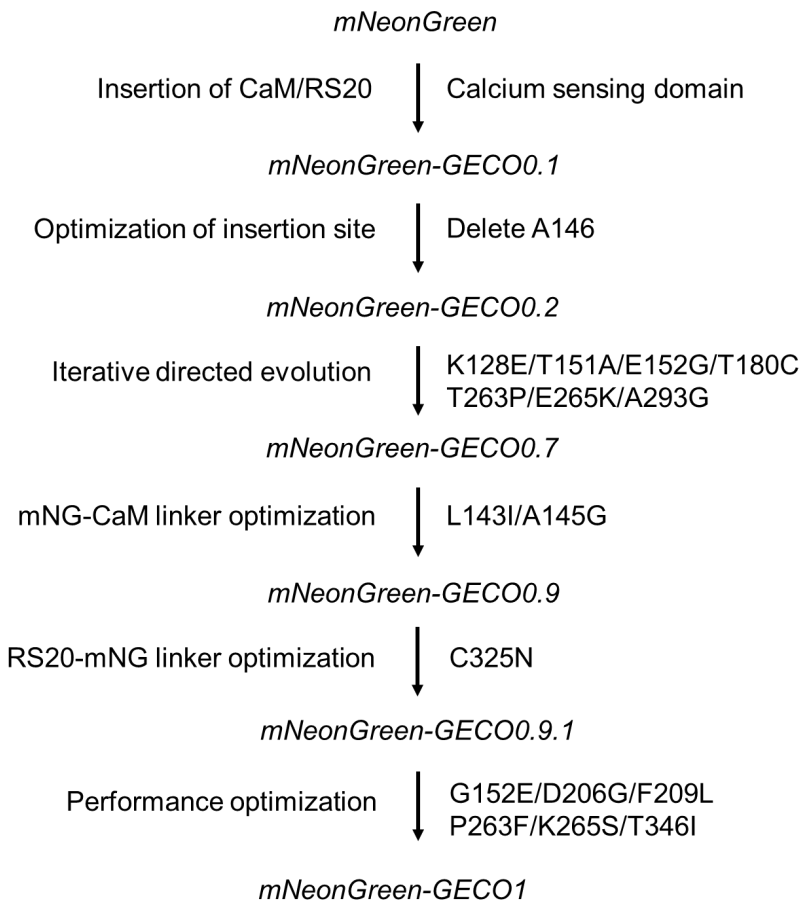

Supplementary Figure 1 Overview of mNG-GECO1 development

Lineage of mNG-GECO variants starting from initial insertion of Ca^{2+} sensing domain into mNG, and ending with the final mNG-GECO1 variant.

```
                                  20                                  40                                  60
mNG-GECO0.1   MVSKGEEDNM ASLPATHELH IFGSINGVDF DMVGQGTGNP NDGYEELNLK STKGDLQFSP 60
mNG-GECO0.2   MVSKGEEDNM ASLPATHELH IFGSINGVDF DMVGQGTGNP NDGYEELNLK STKGDLQFSP 60
mNG-GECO0.7   MVSKGEEDNM ASLPATHELH IFGSINGVDF DMVGQGTGNP NDGYEELNLK STKGDLQFSP 60
mNG-GECO0.9   MVSKGEEDNM ASLPATHELH IFGSINGVDF DMVGQGTGNP NDGYEELNLK STKGDLQFSP 60
mNG-GECO0.9.1 MVSKGEEDNM ASLPATHELH IFGSINGVDF DMVGQGTGNP NDGYEELNLK STKGDLQFSP 60
mNG-GECO1    MVSKGEEDNM ASLPATHELH IFGSINGVDF DMVGQGTGNP NDGYEELNLK STKGDLQFSP 60
                                  80                                 100                                 120
mNG-GECO0.1   WILVPHIGYG FHQYLPYPDG MSPFQAAMVD GSGYQVHRTM QFEDGASLTV NYRYTYEGSH 120
mNG-GECO0.2   WILVPHIGYG FHQYLPYPDG MSPFQAAMVD GSGYQVHRTM QFEDGASLTV NYRYTYEGSH 120
mNG-GECO0.7   WILVPHIGYG FHQYLPYPDG MSPFQAAMVD GSGYQVHRTM QFEDGASLTV NYRYTYEGSH 120
mNG-GECO0.9   WILVPHIGYG FHQYLPYPDG MSPFQAAMVD GSGYQVHRTM QFEDGASLTV NYRYTYEGSH 120
mNG-GECO0.9.1 WILVPHIGYG FHQYLPYPDG MSPFQAAMVD GSGYQVHRTM QFEDGASLTV NYRYTYEGSH 120
mNG-GECO1    WILVPHIGYG FHQYLPYPDG MSPFQAAMVD GSGYQVHRTM QFEDGASLTV NYRYTYEGSH 120
                                 140                                 160                                 180
mNG-GECO0.1   INGEAQVKGT GFPADGPVMT NSLTAATRDQ LTEEQIAEFK EAFSLFDKDG DGTITTKELG 180
mNG-GECO0.2   INGEAQVKGT GFPADGPVMT NSLTA-TRDQ LTEEQIAEFK EAFSLFDKDG DGTITTKELG 179
mNG-GECO0.7   INGEAQVEGT GFPADGPVMT NSLTA-TRDQ LAGEQIAEFK EAFSLFDKDG DGTITTKELG 179
mNG-GECO0.9   INGEAQVEGT GFPADGPVMT NSITG-TRDQ LAGEQIAEFK EAFSLFDKDG DGTITTKELG 179
mNG-GECO0.9.1 INGEAQVEGT GFPADGPVMT NSITG-TRDQ LAGEQIAEFK EAFSLFDKDG DGTITTKELG 179
mNG-GECO1    INGEAQVEGT GFPADGPVMT NSITG-TRDQ LAEEQIAEFK EAFSLFDKDG DGTITTKELG 179
                                 200                                 220                                 240
mNG-GECO0.1   TVLRSLGQNP TEAELQDMIN EVDADGDGTF DFPEFLTMMA RKMNDADSEE EIREAFRVFD 240
mNG-GECO0.2   TVLRSLGQNP TEAELQDMIN EVDADGDGTF DFPEFLTMMA RKMNDADSEE EIREAFRVFD 239
mNG-GECO0.7   CVLRSLGQNP TEAELQDMIN EVDADGDGTF DFPEFLTMMA RKMNDADSEE EIREAFRVFD 239
mNG-GECO0.9   CVLRSLGQNP TEAELQDMIN EVDADGDGTF DFPEFLTMMA RKMNDADSEE EIREAFRVFD 239
mNG-GECO0.9.1 CVLRSLGQNP TEAELQDMIN EVDADGDGTF DFPEFLTMMA RKMNDADSEE EIREAFRVFD 239
mNG-GECO1    CVLRSLGQNP TEAELQDMIN EVDADGGGTL DFPEFLTMMA RKMNDADSEE EIREAFRVFD 239
                                 260                                 280                                 300
mNG-GECO0.1   KDGNGYIGAA ELRHVMTDLG EKLTDEEVDE MIRVADIDGD GQVNYEEFVQ MMTAKGGGGS 300
mNG-GECO0.2   KDGNGYIGAA ELRHVMTDLG EKLTDEEVDE MIRVADIDGD GQVNYEEFVQ MMTAKGGGGS 299
mNG-GECO0.7   KDGNGYIGAA ELRHVMTDLG EKLPDKEVDE MIRVADIDGD GQVNYEEFVQ MMTGKGGGGS 299
mNG-GECO0.9   KDGNGYIGAA ELRHVMTDLG EKLPDKEVDE MIRVADIDGD GQVNYEEFVQ MMTGKGGGGS 299
mNG-GECO0.9.1 KDGNGYIGAA ELRHVMTDLG EKLPDKEVDE MIRVADIDGD GQVNYEEFVQ MMTGKGGGGS 299
mNG-GECO1    KDGNGYIGAA ELRHVMTDLG EKLFDSEVDE MIRVADIDGD GQVNYEEFVQ MMTGKGGGGS 299
                                 320                                 340                                 360
mNG-GECO0.1   VDSSRRKWNK AGHAVRAIGR LSSDWCRSKK TYPNDKTIIS TFKWSYTTGN GKRYRSTART 360
mNG-GECO0.2   VDSSRRKWNK AGHAVRAIGR LSSDWCRSKK TYPNDKTIIS TFKWSYTTGN GKRYRSTART 359
mNG-GECO0.7   VDSSRRKWNK AGHAVRAIGR LSSDWCRSKK TYPNDKTIIS TFKWSYTTGN GKRYRSTART 359
mNG-GECO0.9   VDSSRRKWNK AGHAVRAIGR LSSDWCRSKK TYPNDKTIIS TFKWSYTTGN GKRYRSTART 359
mNG-GECO0.9.1 VDSSRRKWNK AGHAVRAIGR LSSDWNRSKK TYPNDKTIIS TFKWSYTTGN GKRYRSTART 359
mNG-GECO1    VDSSRRKWNK AGHAVRAIGR LSSDWNRSKK TYPNDKTIIS TFKWSYITGN GKRYRSTART 359
                                 380                                 400
mNG-GECO0.1   TYTFAKPMAA NYLKNQPMYV FRKTELKHSK TELNFKEWQK AFTDVMGMDE LYK 413
mNG-GECO0.2   TYTFAKPMAA NYLKNQPMYV FRKTELKHSK TELNFKEWQK AFTDVMGMDE LYK 412
mNG-GECO0.7   TYTFAKPMAA NYLKNQPMYV FRKTELKHSK TELNFKEWQK AFTDVMGMDE LYK 412
mNG-GECO0.9   TYTFAKPMAA NYLKNQPMYV FRKTELKHSK TELNFKEWQK AFTDVMGMDE LYK 412
mNG-GECO0.9.1 TYTFAKPMAA NYLKNQPMYV FRKTELKHSK TELNFKEWQK AFTDVMGMDE LYK 412
mNG-GECO1    TYTFAKPMAA NYLKNQPMYV FRKTELKHSK TELNFKEWQK AFTDVMGMDE LYK 412
```

Supplementary Figure 2 Sequence alignment of mNG-GECO variants

Alignment of mNG-GECO variants 0.2, 0.7, 0.9, 0.9.1, and 1. Similar to the topological representation in **Fig. 1a**, mNG barrel (yellow), CaM (light blue), RS20 (green), linker regions (black), mutations (red), and the chromophore forming residues (black box over "GYG"). Also highlighted are the two residues that flank the insertion site (residue 136 of mNG in purple and residue 139 in magenta; numbering as in PDB ID 5LTR), which are shown as circles in both the protein structure and gene schematic in **Fig. 1a**.

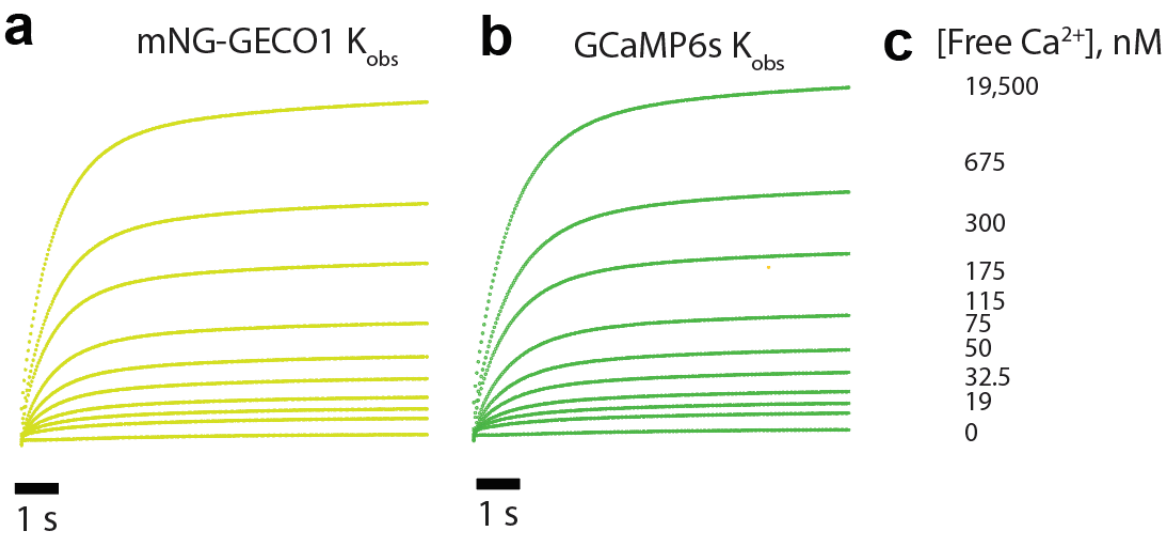

Supplementary Figure 3 K_{on}, (observed) traces of mNG-GECO1 and GCaMP6s purified protein using Photophysics SX-20 Stopped-flow. Each protein buffered in 30 mM MOPS, 100 mM KCl, 50 μM EGTA is rapidly mixed at 1:1 ratio with varying concentrations of Ca^{2+} produced by reciprocal dilutions of 10 mM EGTA and 10 mM CaEGTA. **a** mNG-GECO1 change in fluorescence over time as Ca^{2+} is rapidly mixed. **b** GCaMP6s change in fluorescence over time as Ca^{2+} is rapidly mixed. **c** Final free-Ca^{2+} concentrations produced after reciprocal dilutions. mNG-GECO1 and GCaMP6s fit with a double exponential curve due to a slow rate limiting step likely caused by the conformational change of the proteins upon binding to Ca^{2+}. Both sensors have a similar $t_{1/2}$ for physiologically relevant Ca^{2+} concentrations.

646

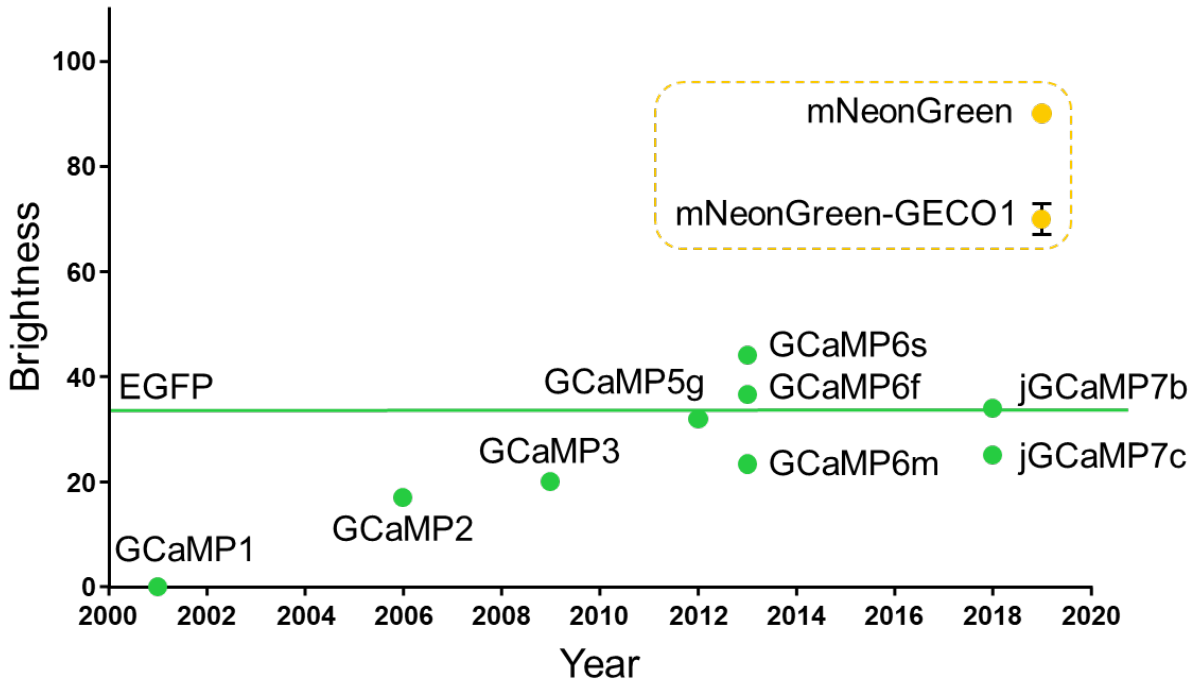

647

648 **Supplementary Figure 4 *In vitro* brightness comparison of mNG-GECO1 to GCaMP series**
649 1P purified protein brightness of first generation mNG-GECO1 compared to the GCaMP series of
650 Ca^{2+} indicators. mNG-GECO1 is substantially brighter *in vitro* than the highly-engineered GCaMP
651 series, which is roughly as bright as its own scaffold, EGFP.

652

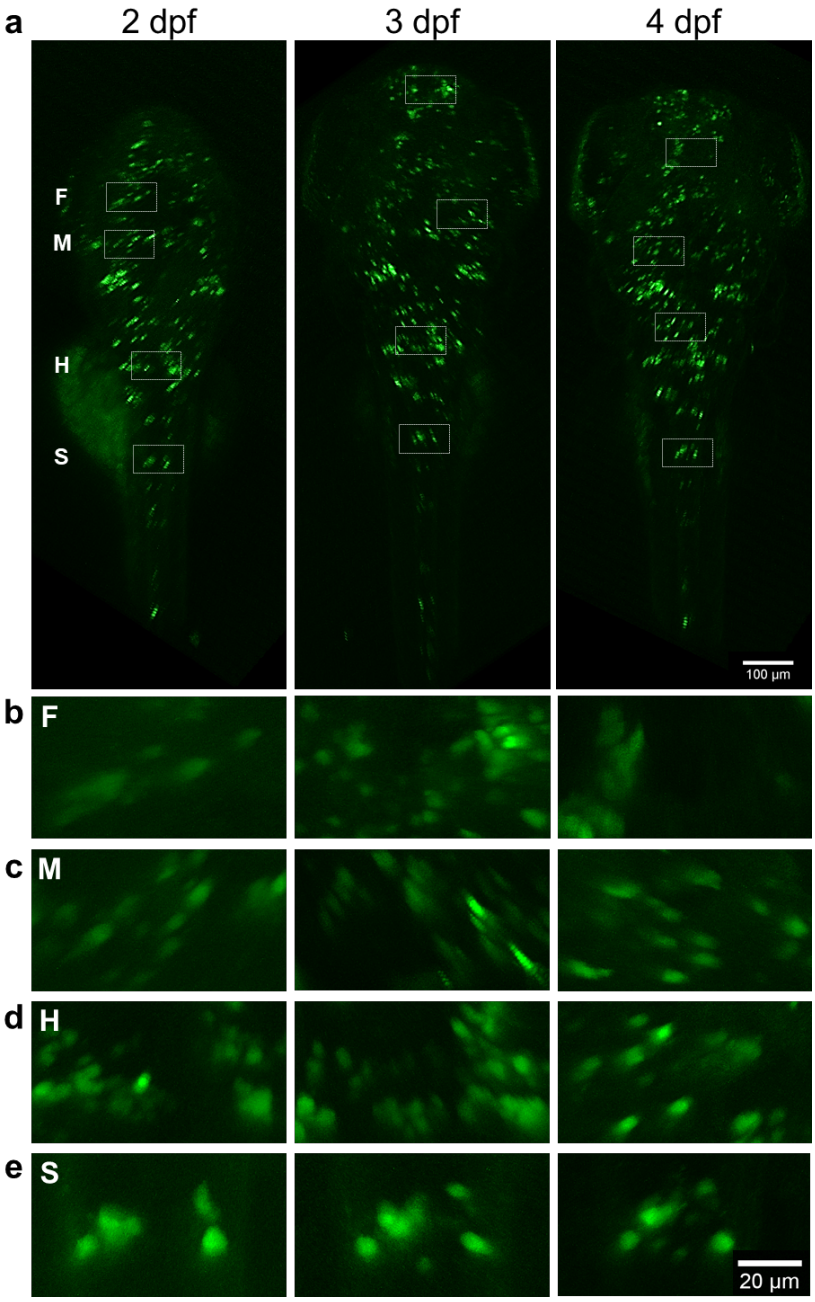

Supplementary Figure 5 mNG-GECO1 expression profile in zebrafish larvae. Transient expression of mNG-GECO1 in Tg[elavl3:mNG-GECO1] zebrafish at 2, 3 and 4 days post-fertilization. **a** Dorsal view of confocal z-projections obtained from the whole larvae. Small dashed squares mark areas that have been enlarged and presented in b-e. **b-e** Shows areas in the forebrain (F), midbrain (M), hindbrain (H) and spine (S). Scale bars are 100 µm in A and 20 µm in b-e as shown bottom right in e.

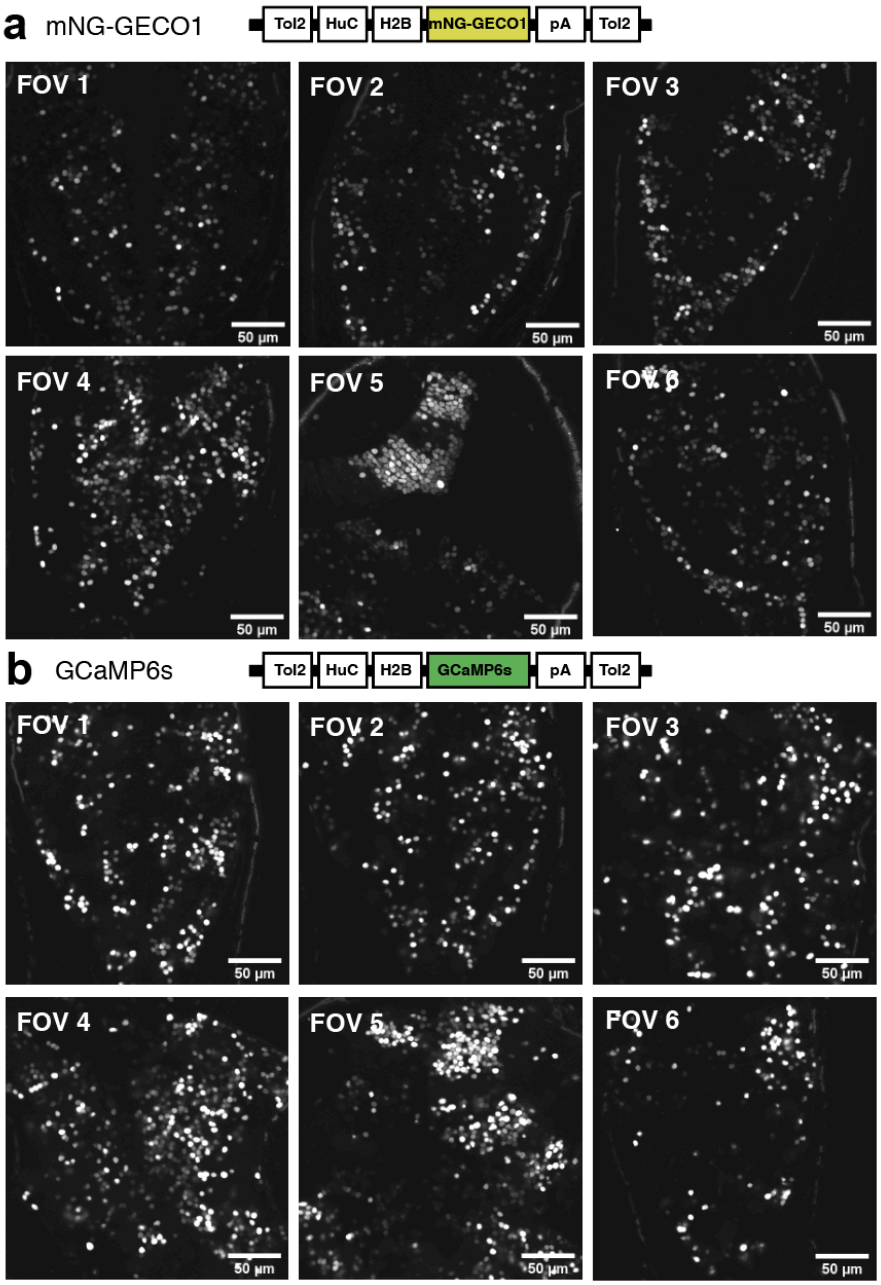

Supplementary Figure 6 mNG-GECO1 and GCaMP6s field of views (FOV) in zebrafish larvae used for quantification. Transient expression of mNG-GECO1 and GCaMP6s in zebrafish at 6 days post-fertilization. Each FOV image is an average intensity of a 5 minute recording encoding 900 frames. The relative fluorescence intensity is to-scale between the two sensors. **a** FOVs from larvae expressing mNG-GECO1. **b** FOVs from larvae expressing GCaMP6s. Scale bar is 50 µM for all images.

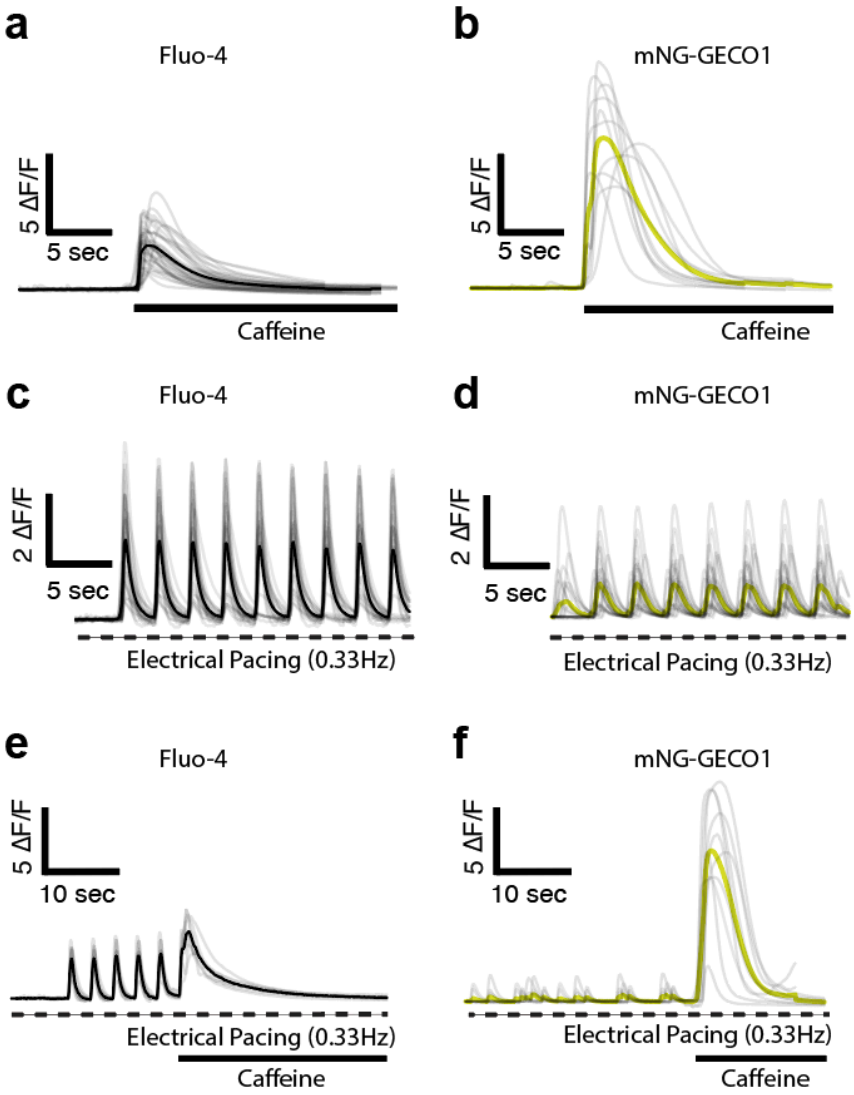

Supplementary Figure 7 Comparison of Fluo-4 Ca^{2+} dye and mNG-GECO1 in human iPSC-derived cardiomyocytes. **a, b** Single cell Ca^{2+} transient traces from iPSC-CM's loaded with the Fluo-4 Ca^{2+} dye (n = 38 regions of interests [ROI's]) or mNG-GECO1 (n=11 ROI's), respectively. Ca^{2+} transients were evoked using 20 mM caffeine. **c, d** Ca^{2+} transients evoked by electrical pacing were recorded with the Fluo-4 Ca^{2+} dye (n = 25 ROI's) or mNG-GECO1 (n = 22 ROI's), respectively. Cells were stimulated electrically at 0.33 Hz and imaged at 10 Hz frame rate. **e, f** Ca^{2+} transients evoked by electrical pacing (0.33 Hz) and caffeine treatment (10 mM) were recorded at 10 Hz with the Fluo-4 Ca^{2+} dye (n = 8 ROI's) or mNG-GECO1 (n = 8 ROI's), respectively.